Color Helium Bubble Flow-Visualization Technique

Zhao Dong,* Wang Zhongqi,† Zhang Xiaodi,* Qin Jialin,* and Lang Xianzhong†
Harbin Aerodynamic Research Institute, Harbin, China

Color helium bubble flow visualization is a new and unique technique. Flow visualization in the wind tunnel using color helium bubbles has recently been achieved at the Harbin Aerodynamic Research Institute. Rich and varied color paths are obtained. This paper describes a unique principle of light interference for flow visualization with color helium bubbles. The different colors of the helium bubbles depend on the wavelength of light, the refractive index and thickness of the bubble film, and the angle of reflection in the bubble film. Methods for controlling these four parameters are indicated. A formula for the bubble film-thickness calculation is derived. The corresponding relation between the bubble film thickness and other parameters is calculated. Typical flow-visualization photographs are presented. An appraisal of the significance of color helium bubble flow visualization is given.

Introduction

HELIUM bubble flow visualization is one of the important visualization techniques of flow patterns around wind-tunnel models. It is well known that a helium-filled bubble generator produces neutrally buoyant bubbles that, when emitted into the freestream forward of the model, will reveal the general flow about the model. A high-intensity light source is placed behind the model and directed upstream such that the bubbles appear white in contrast to the black surfaces of the model and background (wind-tunnel wall). Thus, the stereoscopic flow pattern on wind-tunnel models is clear at a glance.[1] At present, a monochromatic helium bubble flow-visualization technique has been extensively applied to the physical study of flow around wind-tunnel models in many countries.

The monochromatic helium bubble flow visualization was realized in July 1982 at the Harbin Aerodynamic Research Institute. After that, color helium bubble flow visualization was successfully realized in March 1984.

Just as dye lines of different colors have an advantage over the monochromatic ones in a water tunnel, so color helium bubbles are superior to monochromatic ones for flow visualization in wind tunnels. In comparison with color dye lines in a water tunnel, the color helium bubble flow-visualization technique in a wind tunnel can be realized at higher Reynolds numbers. Moreover, for unsteady flowfields, qualitative visualization can be realized and quantitative information can be obtained.[2] As for visual resolution, color helium bubbles are superior to monochromatic ones, so the use of the color helium bubbles can benefit flow-visualization tests in wind tunnels.

Principle of Color Visualization

Different colors of helium bubbles are caused by interference effects of light. Helium bubble film thickness is about 0.5–1μ. The film surface is curved. Thicknesses are not equal in different positions. Thus, the study of light interference phenomenon for helium bubble is complicated.

Suppose a transparent film with plane-reflecting surfaces, not necessarily parallel, is illuminated by a point source S of quasimonochromatic light. Two rays‡ from S, namely SAP and $SBCDP$ (Fig. 1), reach any point P on the same side of the film as S, so that there is a nonlocalized interference pattern in this region. The difference between these two optical paths from S to P is

$$\Delta\varphi = n(SB + DP - SA - AP) + n'(BC + CD) \tag{1}$$

where n' and n are, respectively, the refractive indices of the film and of the surrounding medium.[3] The exact value of $\Delta\varphi$ may be difficult to calculate, but if the film is sufficiently thin, B, A, and D are close together on the upper surface, so that

$$nSA \fallingdotseq nSB + n'BN_1 \tag{2}$$

$$nAP \fallingdotseq nDP + n'N_2D \tag{3}$$

where AN_1 and AN_2 are, respectively, perpendicular to BC and CD. From Eqs. (1–3)

$$\Delta\varphi \fallingdotseq n'(N_1C + CN_2) \tag{4}$$

Further, if the angle between the surfaces of the film is sufficiently small,

$$N_1C + CN_2 \fallingdotseq N_1'C + CN_2' \tag{5}$$

where N_1' and N_2' are, respectively, the feet of perpendiculars from E to BC and CD, and E is the intersection with the upper surface of the normal to the lower surface at C. Now

$$N_1'C = CN_2' = h\cos\theta' \tag{6}$$

where $h = CE$ is the thickness of the film at C, measured normal to the lower surface, and θ' is the angle of reflection in the film. Hence, for a thin film of small angle, we may write from Eqs. (4–6)

$$\Delta\varphi = 2n'h\cos\theta' \tag{7}$$

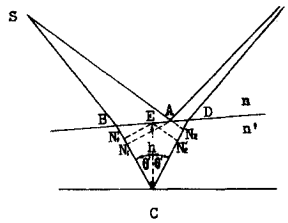

Fig. 1 Thin film with point source.

Presented as Paper 86-1.7.1 at the 15th Congress of the International Council of Aeronautical Sciences, Albuquerque, NM, Sept. 17–19, 1986; received Nov. 13, 1986; revision received June 30, 1987.

*Senior Engineer, Research Department.
†Engineer, Research Department.

‡We neglect multiple reflections.

and the corresponding phase difference at P is

$$\delta = \frac{4\pi}{\lambda_0} n'h \cos\theta' \tag{8}$$

where λ_0 is the wavelength of light.

In general, for a given P, both h and θ' vary with the position of S, and a small extension of the source makes the range of δ at P so large that the fringes disappear. There is, however, a special case when P is in the film, as when observations are made with a microscope focused on the film, or with the eye accommodated for it. Under these circumstances, h is practically the same for all pairs of rays from an extended source reaching P', conjugate to P (Fig. 2), and differences of δ at P' are due mainly to differences of $\cos\theta'$. If the range of value of $\cos\theta'$ is sufficiently small, the range of δ at P' may be much less than 2π even with a source of appreciable extension, and distinct fringes are then visible, apparently localized in the film. In practice, the condition of a small range of $\cos\theta'$ can be satisfied by observing near-normal incidence, and also by the fact that the pupil of the unaided eye is itself sufficiently small. If we take into account the phase change of π on reflection at one of the surfaces of the film, there are maxima of intensity at P' (and so apparently at p) when

$$2n'h\,\overline{\cos\theta'} \pm \frac{\lambda_0}{2} = \lambda_0 m = 0, 1, 2, \ldots \tag{9}$$

and minima of intensity when

$$2n'h\,\overline{\cos\theta'} \pm \frac{\lambda_0}{2} = m\lambda_0 m = \frac{1}{2}, \frac{3}{2}, \frac{5}{2}, \ldots \tag{10}$$

where $\overline{\cos\theta'}$ is a mean value of $\cos\theta'$ for the points of the source that contribute light to P'. The quantity $n'h$ that appears in these relations is the optical thickness of the film at P; as far as our approximations are concerned, the state of interference at P is unaffected by the film thickness elsewhere. It follows that Eqs. (9) and (10) hold even if the bounding surfaces of the thin film are not plane, so long as the angle between them remains small. If a source of white light is used, the interference fringes of surface for helium bubble are colored ones.

Method of Color Visualization

From (7) and (8), the different colors of color helium bubbles are dependent on n', h, θ', and λ_0. In reality, the key to the color helium bubble flow-visualization technique lies in control of these four parameters.

As for the light source, first, the intensity of light must be high enough; second, this technique requires as wide a wavelength region as possible to achieve rich and varied colors. The color light source that was used in this study can satisfy the need of color helium bubble flow visualization. We have employed a dysprosium arc lamp with 1000 W to light the bubbles. This lamp has some broadband wavelengths.

Only some specific refractive indices of film can obtain the different colors, and so only a part of the bubble film solution is suitable for the appearance of color. In fact, our bubble film solution (such as BFS 1110, 1120, 2115, and 4120) used with the monochromatic helium bubble flow visualization did not produce colors. By use of the color bubble film solution CPY 240-3 developed at the Harbin Aerodynamic Research Institute, rich and varied colors were obtained. The bubble generation rate was increased substantially over what had been obtained previously. Furthermore, the solution is not toxic, corrosive, or likely to stain anything.

The angle of reflection in the film must be confined within necessary limits. If the range of θ' is too large, various colors will appear for a certain bubble in different positions. If so, the different bubble paths cannot be distinguished by color. Thus, the relative position of the color light source, model, and head must be arranged reasonably. The distance between the light source and the model must be long enough. It was greater than 1.5 m in this study.

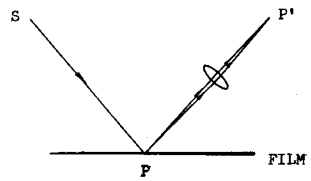

Fig. 2 Thin film: illustrating formation of fringe localized in the film.

The color helium bubble flow-visualization technique requires the film-thickness distribution to be wide enough to obtain rich and varied colors. For this reason, the control of the film thickness h is important. This is discussed in the next section.

Calculation and Control of Bubble Film Thickness

Since the bubbles are filled with helium and thus neutrally buoyant, they will follow flow quite well. As a consequence, at neutral buoyancy the weight of the helium bubble should equal that of air with the same volume, i.e.,

$$\gamma_B v_B + \gamma_H v_H = \gamma_K v_K \tag{11}$$

where γ is specific gravity and v volume. The subscripts B, H, and K indicate the bubble film solution, helium, and air, respectively. If we assume that the helium bubble is a spherical shape, Eq. (11) can be written in the form

$$\frac{4\pi}{3}[r^3 - (r-h)^3]\gamma_B + \frac{4\pi}{3}(r-h)^3\gamma_H = \frac{4\pi}{3} r^3 \gamma_K \tag{12}$$

where r is the radius of the helium bubble and h the thickness of the film. After the substitution of γ_B, γ_H, and γ_K in Eq. (12) and simplifying, one has

$$Ah^3 - Brh^2 + Cr^2h - Dr^3 = 0 \tag{13}$$

where A, B, C, and D are constants. From Eq. (13), one can find the relation between h and r. With r as an independent variable, Eq. (13) is a simple cubic equation. First, in the numerical calculation, the approximate solution h_0 is found by using a numerical-graphic method to approximate quickly the exact solution h. If we assume that the exact solution of the film thickness is $h_0 + \Delta h$, i.e., $h = h_0 + \Delta h$, then Eq. (13) can be written in the form

$$f(h_0 + \Delta h) = 0 \tag{14}$$

In order to be able to determine Eq. (14) by the use of the Taylor formula, we expand the left side in the power series

$$f(h_0 + \Delta h) = f(h_0) + f'(h_0)\,\Delta h + \frac{f''(h_0)}{2!}\Delta h^2 + \cdots + \frac{f^{(n+1)}_{(h_0)}}{(n-1)!}\Delta h^{n-1} + \frac{f^{(n)}_{(c)}}{n!}\Delta h^n \tag{15}$$

where $h \gtrless c \gtrless h_0 + \Delta h$. Since Δh is very small, terms of second degree and higher in Δh can be omitted from Eq. (15). Thus,

$$f(h_0 + \Delta h) = f(h_0) + f'(h_0)\Delta h = 0 \tag{16}$$

and hence,

$$\Delta h = -\frac{f(h_0)}{f'(h_0)} \tag{17}$$

where

$$f(h_0) = Ah_0^3 - Brh_0^2 + Cr^2h_0 - Dr^3 \quad (18)$$

$$f'(h_0) = 3Ah_0^2 - 2Brh_0 + Cr^2 \quad (19)$$

After Δh, the film thickness $h_1 = h_0 + \Delta h$ can be calculated. After this, replace h_0 by h_1 in order to conduct an approximate calculation for the second time. In general, $\Delta h < 10^{-7}$ mm can be achieved by double approximation. When calculating h corresponding to other r, one need not again apply the numerical-graphic method. The approximate solution h corresponding to some r can be obtained from a known h near to this r.

The calculated result for the relation between the film thickness and the bubble diameter is shown in Fig. 3. It can be seen that the relation between h and d is linear. In practice, one can control the film thickness by controlling the diameter of the bubble. Hence, one can obtain the requisite film thickness by controlling the parametric distributions of compressed air, helium, and bubble film solution.

At some instant, the bubble diameter distribution is not uniform. In a typical experimental condition, the rate of bubbles generated per second is shown in Table 1. Here, it can be seen that the diameters are different. When the parameters associated with compressed air, helium, and bubble film solution are kept constant, there are various size bubbles generated. Of course, the film thicknesses of the bubbles are different, too (see Table 2). Thus, different colors are ensured.

Testing Installation

Motion for the head of the bubble generator was made using a traverse device mounted on top of the wind tunnel (Fig. 4). The traverse device has a vertical traverse of 800 mm and an azimuthal traverse of 90 deg and a longitudinal traverse of 1000 mm, so the head mounted in the stem holder can be placed in a suitable place for flow visualization.

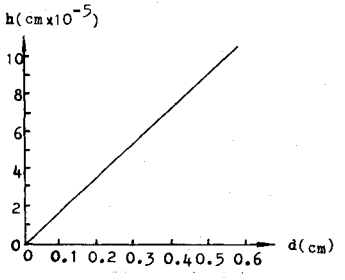

Fig. 3 Corresponding relation between the film thickness and the diameter of bubble.

Table 1 Parameters of generated bubbles

Diameter, cm	Bubbles/s	Percentage, %
0.5	46	11.5
0.4	44	11
0.2, 0.3	256	65
0.1	50	12.5

Table 2 Film thickness of generated bubbles

Diameter, cm	Film thickness, cm
0.1	1.847×10^{-5}
0.2	3.679×10^{-5}
0.3	5.547×10^{-5}
0.4	7.395×10^{-5}
0.5	9.245×10^{-5}

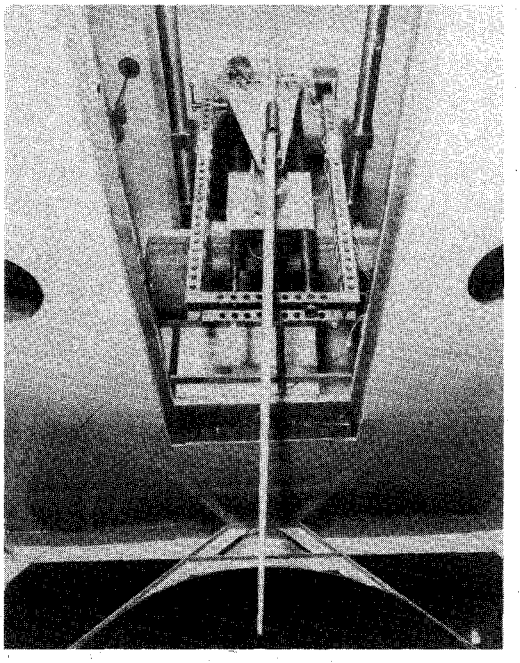

Fig. 4 Traverse device.

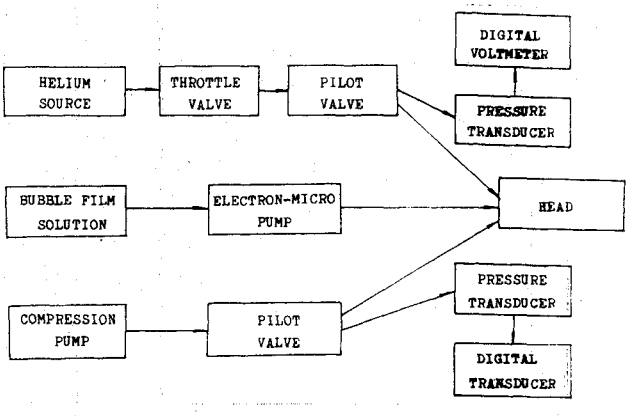

Fig. 5 Flowchart of the bubble generator.

Figure 5 shows a flowchart of the bubble generator. Pressure of the helium source is 150 kg/cm^2; it is reduced to 5 kg/cm^2 using a throttle valve. After that, the helium pressure is regulated to the working pressure of the head by a pilot valve. The working pressure is transmitted to a pressure transducer that is connected to a digital voltmeter. Value of the working pressure is displayed on the digital volt-meter.

Maximum output pressure of the compression pumb is 7 kg/cm^2. The regulation and display of the air pressure are similar to those of the helium pressure.

The bubble film solution is supplied to the head of the bubble generator by an electron-micro pump. The large-capacity electron-micro pump has a flow capacity of 4.8–18 ml/min, and the small-capacity one a flow capacity of 0.12–4.2 ml/min.

Typical Flow-Visualization Photographs

Figures 6–9 present photographs of the color helium bubble flow visualization of a 1/21-scale YF-16 model. The wind tunnel is a low-speed open-return tunnel. The test section has a diameter of 1500 mm and a length of 1950 mm. The wind tunnel is operated at a test-section velocity of 10 m/s. Figures 6–9 present results obtained for $\alpha = 14$ and 8 deg, respectively, where α is the angle of attack. Figures 7 and 8 present patterns of the strake vortex and of the wing leading-edge vortex. Figures 6 and 9 show patterns of the latter half of the strake vortex and of the outside vortex.

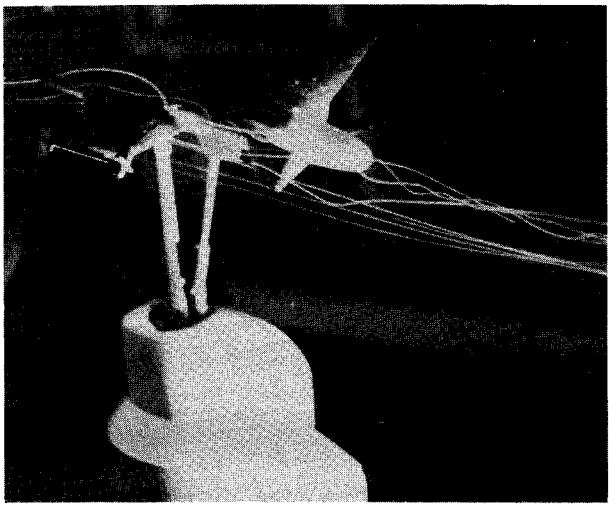

Fig. 6 Pattern of the latter half of the strake vortex.

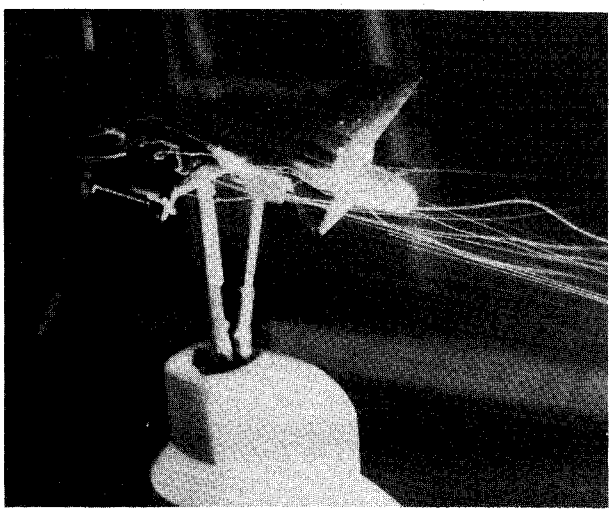

Fig. 8 Patterns of vortex nucleus of the strake vortex and wing leading edge vortex.

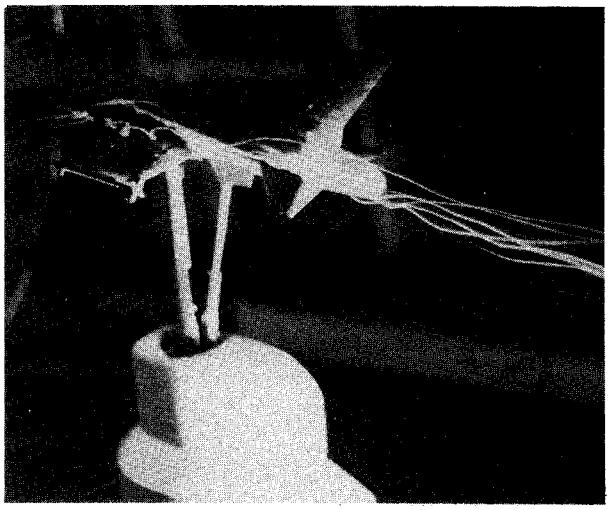

Fig. 7 Patterns of the strake vortex and wing leading edge vortex.

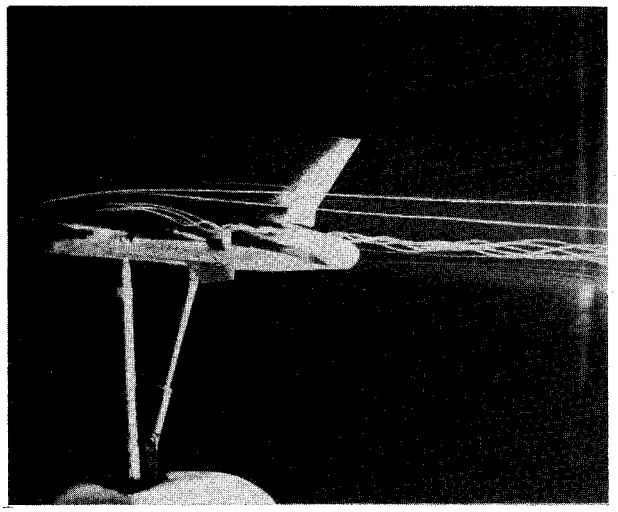

Fig. 9 Patterns of the latter half of the strake vortex and outside vortex.

From these photographs it can be seen that color helium bubbles are superior to the monochromatic ones for flow visualization. The stream lines associated with the different colors can be resolved easily, especially when many stream lines are in close proximity. Thus, for complex three-dimensional flowfields, the color helium bubble flow-visualization technique is very useful, whether for qualitative visualization or for quantitative measurement.

Conclusions

Flow visualization using color helium bubbles in a wind tunnel is a new and unique technique. Emergence of this technique makes stereoscopic and color flow visualization possible in air. Moreover, in comparison with the color dye lines in a water tunnel, flow visualization can be realized at higher Reynolds numbers. Finally, for unsteady flowfields, the qualitative visualization can be realized and the quantitative information obtained.

The color bubble film solution that was developed using a color light source and the method of color visualization presented ensures reasonable values of λ_0, n', h, and θ'. Rich and varied color helium bubble paths were obtained. The visual resolution on varied paths increased greatly. Clear color video taperecording and color photographs were possible. Thus, the color helium bubble flow-visualization technique is important, whether for qualitative visualization or quantitative measurement.

References

[1]Hale, R. W., Tan, P., Stowell, P. C., and Ordway, D. E., "Development of an Integrated System for Flow Visualization in Air Using Neutrally-Buoyant Bubbles," AD-756691, Dec. 1971.

[2]Rogers, D.. F., "Quantitative Information from Helium Bubble Flow Visualization Using Computer Graphics Techniques," AIAA Paper 76-93, Jan. 1976.

[3]Born, M. and Wolf, E., *Principles of Optics*, 5th ed., Pergamon Press, New York, 1975, pp. 286–287.